

1 **Investigation of an extreme rainfall event during 8–12 December 2018 over central**
2 **Viet Nam – Part 2: An evaluation of predictability using a time-lagged cloud-resolving**
3 **ensemble system**

4 Chung-Chieh Wang¹, Duc Van Nguyen^{1,2}, Thang Van Vu², Pham Thi Thanh Nga², Pi-Yu
5 Chuang¹, and Kien Ba Truong^{2,*}

6 Correspondence: kien.cbg@gmail.com

7 ¹Department of Earth Sciences, National Taiwan Normal University, Taipei, Taiwan

8 ²Viet Nam Institute of Meteorology, Hydrology and Climate Change, Hanoi, Viet Nam

9 **Abstract:**

10 This is the second part of a two-part study that investigates an extreme rainfall event that
11 occurred from 8 to 12 December 2018 over central Viet Nam (referred to as the D18 event).
12 In this part, the study aims to evaluate the practical predictability of the D18 event using
13 the quantitative precipitation forecasts (QPFs) from a time-lagged cloud-resolving
14 ensemble system. To do this, 29 time-lagged (8 days in forecast range) high resolution (2.5
15 km) members were run, with the first member initialized at 12:00 UTC 3 December and
16 the last one at 12:00 UTC 10 December 2018. Between the first and the last members are
17 multiple members that were executed every 6 h. The evaluation results reveal that the
18 cloud-resolving model (CReSS) well predicted the rainfall fields at the short range (less
19 than 3 days) for 10 December (the rainiest day). Particularly, the CReSS shows high skill
20 in heavy-rainfall QPFs for this date with a Similarity Skill Score (SSS) greater than 0.5 for
21 both the last five members and the last nine members. The good results are due to the model
22 having good predictions of relevant meteorological variables such as surface winds.
23 However, the predictive skill is reduced at lead times longer than 3 days, and it is
24 challenging to achieve good QPFs for rainfall thresholds greater than 100 mm at lead times
25 longer than 6 days. These results also confirmed our scientific hypothesis that the cloud-
26 resolving time-lagged ensemble system (using the CReSS model) improved the QPFs of

this event at the short range. Furthermore, the results also demonstrated that a decent QPF can be made at a longer lead time (by a member initialized at 1800 UTC 4 December).

In addition, the ensemble-based sensitivity analysis (ESA) of 24-h rainfall in central Viet Nam shows that it is highly sensitive to initial conditions, not only at lower levels but also at upper levels. The rainfall is sensitive to both kinematics and moisture convergence at low levels, and such sensitivities decrease with increasing lead time. The ESA also facilitates a better understanding of the mechanisms in the D18 event, implying that it is meaningful to apply ESA to control initial conditions in the future.

1 Introduction

The present study is the second part of a two-part study investigating the extreme rainfall event during 8–12 December 2018 over central Viet Nam (referred to as the D18 event hereafter). In this event, record-breaking rainfall occurred along the mid-central coast of Viet Nam, from Quang Binh to Quang Ngai provinces. The observation shows that the peak amount in rainfall accumulation, in particular, exceeded 800 mm over a 3-day period from 12:00 UTC 8 to 12:00 UTC 11 December (Fig. 1f). During this period, the rainiest day was 10 December with 24-h observed amount exceeding 600 mm at some stations (Fig. 4 OBS). This record-breaking rainfall event led to 13 deaths, widespread destructions in the environment and downstream cities, and heavy economic losses due to catastrophic flooding and landslides (Tuoi Tre news, 2018). In part 1 (Wang and Nguyen 2023), we focused on the analysis of the mechanism that caused this event and evaluated the simulation by the Cloud-Resolving Storm Simulator (CReSS; Tsuboki and Sakakibara, 2002, 2007). The analysis results point out the main factors which led to this event as well as its spatial rainfall distribution. These factors included the combined interaction between the strong northeasterly winds and easterly winds over the South China Sea (SCS) in the lower troposphere (below 700 hPa). The local terrain also played essential role due to its barrier effect. The cloud model's good simulation results in part 1 indicated its promising potential in forecasting this event. Hence, in part 2, the present study focuses on an

54 evaluation of its predictability of the D18 event through a series of time-lagged high-
55 resolution ensemble quantitative precipitation forecasts (QPFs) by the CReSS model.

56 Predicting heavy rainfall events is still challenging to meteorologists and weather
57 forecasters, although great progresses have been made in the science of numerical weather
58 prediction. The prediction of heavy to extreme rainfall is more difficult for Viet Nam,
59 where both multi-scale interactions among different weather systems and strong influence
60 by local topography often exist. For example, when D18 event occurred, several
61 operational models were unable to predict this event successfully. Specifically, Fig. 1
62 shows the predictions for the D18 event by three global models at the National Centers for
63 Environmental Prediction (NCEP), the European Centre for Medium-Range Weather
64 Forecasts (ECMWF), and the Japan Meteorological Agency (JMA), and by one mesoscale
65 regional model, the Weather Research and Forecasting (WRF) model, implemented for
66 operation at the Mid-central regional Hydro-Meteorological center in Da Nang city, Viet
67 Nam, with the finest horizontal grid spacing (Δx) of $6 \text{ km} \times 6 \text{ km}$. While these models
68 overall made good predictions in the surface wind field, their 72-h accumulated rainfall
69 amounts along the coast of central Viet Nam were less than 250 mm and much lower than
70 the observation, which exceeded 900 mm (Fig. 1). Therefore, in order to improve the QPFs
71 for heavy rainfall events in Viet Nam, we need to not only understand their mechanisms of
72 occurrence, but also adopt or develop better forecasting tools, more effective strategy, or
73 both.

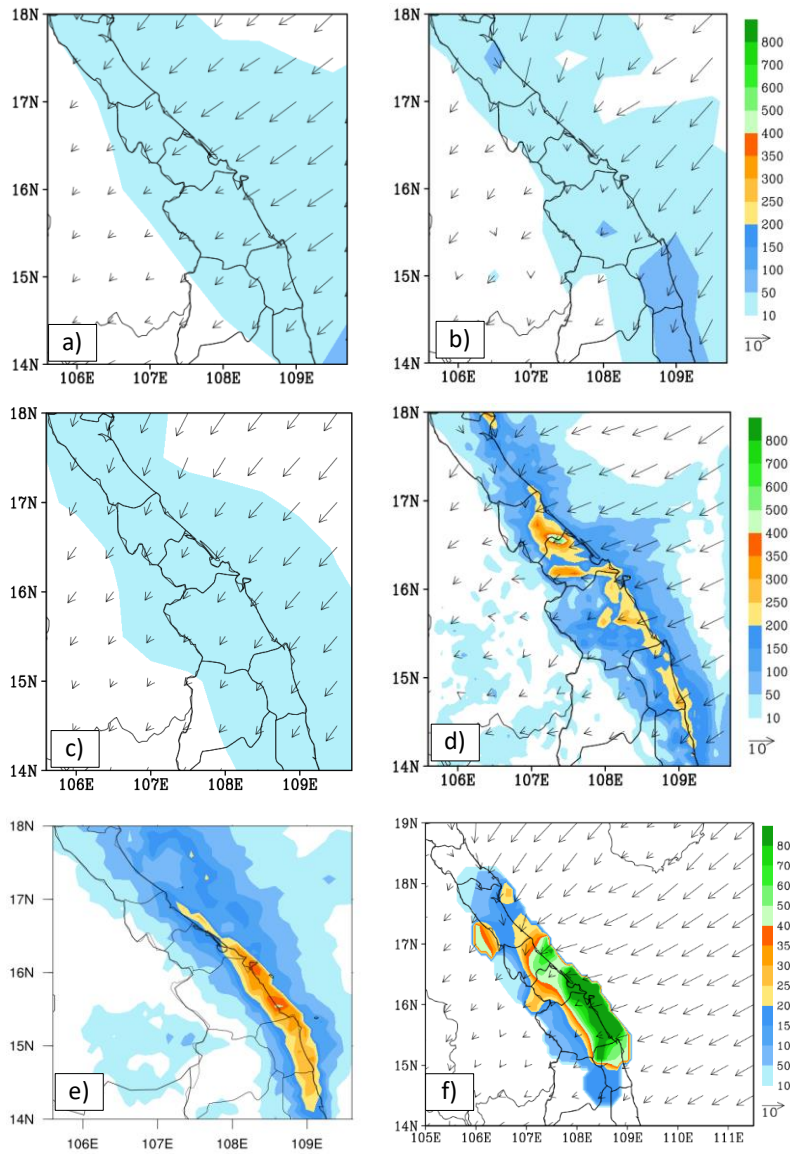


Figure 1. The predicted 72h accumulated rainfall (mm, shaded) and mean surface wind (ms⁻¹, vector) for the period of 12:00 UTC 8 December – 12:00 UTC 11 December 2018 obtained by (a) NCEP, (b) ECMWF, (c) JMA, (d) WRF, (e) 72h accumulated rainfall obtained by the Global Precipitation Measurement (GPM) estimate (IMERG Final Run

product) and (f) 72h in-situ observed accumulated rainfall (mm, shaded) and the mean surface wind derived from ERA5 data (ms^{-1} , vector), adapted from Fig. 14c of Wang and Nguyen (2023).

Among several different methods, present-day weather forecasts depend mainly on numerical weather prediction (NWP) using models, a scientific method that ~~has become indispensable for its ability to~~ simulate weather and produce quantitative results (Fig. 1). However, there is always uncertainty in numerical forecasts due to the fact that the atmosphere is a chaotic system and tiny errors in the initial state can grow rapidly and lead to larger errors in the forecast (Hohenegger and Schär, 2007, Lorenz 1969). Various approximations in numerical methods are also sources of forecast uncertainty. Thus, by generating a range of possible weather conditions in days ahead or into the future, the ensemble forecasting was introduced as an effective method to estimate forecast uncertainty and improve the overall accuracy and usefulness of NWP products. This is because the ensemble mean typically has smaller errors than individual members, since the high predictability features that the members agree on are emphasized by the mean, while the low-predictability ones that the members do not agree on are filtered out or dampened (e.g., Leith 1974; Murphy 1988, Surcel et al. 2014). ~~However, it may smooth out extreme events and underestimate their magnitude.~~ Furthermore, some studies have shown high skill in QPFs for extreme rainfall produced by typhoons in Taiwan using the CReSS model, a cloud-resolving model (CRM), with high resolution and time-lagged approach (Wang et al. 2016; Wang 2015; Wang et al. 2014; Wang et al. 2013). Table 1 of Wang et al. (2016) shows that the high-resolution time-lagged ensemble forecasts provide overall better quality in comparison with both the traditional low-resolution ensemble forecasts and high-resolution deterministic forecasts at a comparable cost in computation.

Besides the advantages of ensemble forecasts described above, the ensemble-based sensitivity analysis (ESA) also provides an effective method to investigate how sensitive the forecast variables are and to what preceding factors. To be more specific, Torn and Hakim (2009) used ESA to evaluate how their subject, a group of tropical cyclones (TCs)

undergoing extratropical transition, in the prediction respond to changes in the initial condition. In their results, the cyclone minimum sea-level pressure forecasts are determined as strongly sensitive to TC intensity and position at short lead times and equally sensitive to mid-latitude troughs that interacted with the TC at longer lead times. For an extreme rainfall event in northern Taiwan, Wang et al. (2021) performed ESA using the results from 45 forecast members with grid sizes of 2.5–5 km to identify contributing factors to heavy rainfall. By normalizing their impacts on rainfall using standard deviation (SD), different factors can be compared quantitatively and on an equal footing. Ranked by their importance, these factors included the position of the surface Mei-yu front and its moving speed, the position of 700-hPa wind shift line and its speed, the moisture amount in the environment near the front, timing and location of frontal mesoscale low-pressure disturbance, and frontal intensity. Many other studies also used the ESA to study TCs, convective events, or support the development of operational ensemble sensitivity-based techniques to improve probabilistic forecasts (e.g., Kerr et al. 2019, Hu and Wu 2020, Coleman and Ancell 2020).

While ensemble-based sensitivity analysis provides valuable insights into key drivers of forecast outcomes as reviewed above, its effectiveness is inherently tied to the limits of predictability, [which can vary by scale \(Surcel et al. 2014, Surcel et al. 2015 and the references therein\)](#). Generally, the atmospheric predictability can be categorized into two types: practical predictability and intrinsic predictability (Melhauser and Zhang 2012, Nielsen and Schumacher 2016, Ying and Zhang 2017, Weyn and Durran 2018). Intrinsic predictability represents the highest achievable predictability using a nearly perfect initial conditions and a nearly perfect forecast model, and is mainly depended on scale and types of weather systems. Whereas, practical predictability describes the predictability using the best-available techniques and initial conditions, and therefore it can be limited by uncertainties in both the model and initial conditions. According to the studies cited above, practical predictability can be improved by improving the initial conditions, but it however

cannot exceed the intrinsic predictability (Ying and Zhang 2017). Based on these, in our study, we investigate the practical predictability of the D18 event because it is a real event.

For heavy precipitation over central Viet Nam, Son and Tan (2009) used the Mesoscale Model version 5 (MM5) to investigate the predictability of heavy-rainfall events over the southern part of central Viet Nam during the period of 2005 and 2007. In this study, experiments were configured for two nested domains with Δx of 27 and 9 km, respectively. Their results showed that the MM5 can predict heavy rainfall there and its performance is better for events caused by TCs or TC interactions with the cold air. Toan et al. (2018) assessed the predictability of heavy rainfall events in middle-central Viet Nam due to combined effects of cold air and easterly winds using the WRF model within a forecast range of 2 days. The model was also set with two nesting domains. The outer domain (D1) covers the entire Vietnam and SCS with a Δx of 18 km, while the inner domain (D2) focuses on the Mid-Central Vietnam region with a Δx of 6 km. The evaluation indicated that at 24-h lead time, the model performed reasonably well at rainfall thresholds less than 100 mm day⁻¹. At the 48-h forecast range, the model performed well only at thresholds below 50 mm day⁻¹ and had some skill at 50–100 mm day⁻¹. However, heavy-rainfall events at thresholds over 100 mm day⁻¹ were almost unpredictable by the model.

Nhu et al. (2017) also used the WRF model to investigate the role of the topography in central Viet Nam on the occurrence of a heavy-rainfall event there in November 1999. In this study, the model with triply-nested domains with Δx of 45, 15, and 5 km and 47 vertical levels well simulated the northeast monsoon circulation, TCs, and the occurrence of heavy rainfall in central Viet Nam. Furthermore, when the topography is removed, the three-day total accumulated rainfall decreased sharply by approximately 75% compared to that in the control experiment with the terrain.

Hoa Van Vo (2016) examined the predictability of heavy-rainfall events during the wet seasons of 2008–2012 in the middle section and central highlands of Viet Nam using NWP products from several global models, including the Global Forecasting System (GFS) of

162 NCEP, Global Spectral Model (GSM) of JMA, Navy Operational Global Atmospheric
163 Processing System (NOGAPS) of the US Navy, and the Integrated Forecast System (IFS)
164 of ECMWF. Their results indicated that the IFS and GSM performed better than the GFS
165 and NOGAPS, and the IFS was evaluated the best. However, all four global models under-
166 estimated rainfall in extreme events. One of the reasons for this under-estimation is that
167 these models are global models, so their resolutions are too coarse for the relatively small
168 study area.

169 The review above suggests that considerable limitations still exist in forecasting heavy
170 rainfall in central Viet Nam, especially using coarser models. It also indicates that a high-
171 resolution time-lagged ensemble approach may offer some advantages in the prediction of
172 extreme rainfall events, such as a better simulation of local weather conditions, a quicker
173 response to changes in forecast uncertainty in real time, and potentially a longer lead time
174 for hazard preparation. Climatologically, the entire Viet Nam lies in the tropical zone (Fig.
175 2a), where vigorous but less organized convection often develops in response to local
176 conditions. This region is also prone to the influence and interactions of weather systems
177 spanning a wide range of scales as reviewed. In addition, although central Viet Nam is a
178 small region with the narrowest place only about 80 km in width, it possesses significant
179 topography running in the north-south direction to affect rainfall (Fig. 2a). Hence, a high-
180 resolution CRM with detailed and explicit treatment in cloud microphysics is likely crucial
181 for better QPFs for heavy rainfall in central Viet Nam.

182 Given the above review and analysis, the scientific hypotheses are proposed: Storm-scale
183 processes and convection were important in the D18 event. However, both global and
184 mesoscale models with a grid size down to $6\text{ km} \times 6\text{ km}$ are not good enough for heavy-
185 rainfall QPF without cloud-resolving capability (Fig. 1). Therefore, it is hypothesized that
186 at higher resolution, the cloud-resolving time-lagged ensemble system (using the CReSS
187 model) can improve the QPFs of this event at the short range. Additionally, this approach
188 may also be able to extend the lead time of decent QPF beyond the short range. So, the
189 goals of the study are to: 1) examine the hypothesis above, 2) investigate the (practical)

predictability of this event through a series of time-lagged ensemble predictions, including whether a decent QPF can be made at a longer lead time, and 3) identify important factors leading to this event, including the lead time of the signals of these factors, using the ESA method. The rest of this paper is organized as follows. Section 2 describes the data, model, and methodology used in the study. The model results are presented and evaluated in Section 3. Finally, conclusions are offered in Section 4.

2 Data and methodology

2.1 Data

2.1.1 Model validation

2.1.1.1 In-situ observation data

The daily in-situ rainfall observations (12:00–12:00 UTC, i.e., 19:00–19:00 LST) from 8 to 12 December 2018 at 69 automated gauge stations across central Viet Nam are used for case overview and verification of model results. This dataset is provided by the Mid-Central Regional Hydro Meteorological Center, Viet Nam. The spatial distribution of these gauge stations is depicted in Fig. 2b.

2.1.1.2 The Global Precipitation Measurement (IMERG Final Run V07) data

The Global Precipitation Measurement (GPM) is a joint international mission between the National Aeronautics and Space Administration (NASA) and the Japan Aerospace Exploration Agency (JAXA), employing a satellite network for advanced global rain and snow observations. The GPM *IMERG Final Run* is a research-level product which is created by intercalibrating, merging, and interpolating “all” satellite microwave precipitation estimates along with microwave-calibrated infrared (IR) satellite estimates, analyses from precipitation gauges, and potentially other precipitation estimation methodologies at fine spatial and time scales. The horizontal resolution of this dataset is $0.1^\circ \times 0.1^\circ$ latitude–longitude and the time interval is every 30 minute (Huffman et al. 2020). In this study, we used this satellite data (version 7) to verify rainfall distribution

216 over the coastal sea due to the limitation of the gauge network, where observations exist
217 only inland as shown in Fig. 2b. The GPM IMERG data span from 12:00 UTC 8 to 12:00
218 UTC 11 December 2018 and are used to analyze the D18 event as well as the rainiest day
219 of this event (10 December).

220 2.1.1.3 The NCEP GDAS/FNL global tropospheric analyses data

221 The present study used this dataset (version d083003) to verify initial data and model
222 outputs. The NCEP FNL analysis is an operational global gridded analysis and is freely
223 provided by the NCEP. The horizontal resolution of this dataset is $0.25^\circ \times 0.25^\circ$ latitude–
224 longitude with 26 levels extending from the surface to 10 hPa. The temporal interval is 6
225 h. The variables used in this study include the zonal and meridional wind components,
226 relative humidity, and vertical velocity at 925 hPa covering the case period from 18:00
227 UTC 4 to 12:00 UTC 9 December 2018.

228 2.1.2 The added values of CReSS ensemble

229 2.1.2.1 The International Grand Global Ensemble retrieval

230 In this study, we used the global model predictions to analyze the predictability of the D18
231 event. The International Grand Global Ensemble (TIGGE) ~~retrieval~~ is a key component of
232 The Observing System Research and Predictability Experiment (THORPEX) research
233 program, whose aim is to accelerate the improvements in the accuracy of 1-day to 2-week
234 high-impact weather forecasts. The TIGGE ~~retrieval~~ provides not only deterministic
235 forecast data but also ensemble prediction datasets from major centers, including NCEP of
236 the USA, ECMWF of the European countries, and JMA of Japan, since 2006. This dataset
237 has been used for a wide range of research studies on predictability and dynamical
238 processes. the variables utilized included total precipitation and surface winds (at 10-m
239 height) from NCEP, ECMWF, and JMA at 6-h intervals during the data period from 12:00
240 UTC 8 to 12:00 UTC 11 December 2018 (as shown in Figs. 1a-c). The link to this dataset
241 is placed in the “code and data availability” section.

242 2.2.1 Model description and experiment setup

243 We used the Cloud-resolving Storm Simulator (CReSS) developed by Nagoya University,
244 Japan (Tsuboki and Sakakibara, 2002, 2007). This is a non-hydrostatic and compressible
245 cloud model, designed for simulation of various weather events at high (cloud-resolving)
246 resolution. In the model, the cloud microphysics is treated explicitly at the user-selected
247 degree of complexity, such as the bulk cold-rain scheme with six species: vapor, cloud
248 water, cloud ice, rain, snow, and graupel (Lin et al., 1983; Cotton et al., 1986; Murakami,
249 1990, 1994; Ikawa and Saito, 1991). Other subgrid-scale processes parameterized, such as
250 turbulent mixing in the planetary boundary layer and physical options for surface
251 processes, including momentum/energy fluxes, shortwave and longwave radiation, are
252 summarized in Table 1.

253 For the initial and boundary conditions (IC/BCs), the NCEP GFS analyses and
254 deterministic forecast runs, executed every 6 h at 00:00, 06:00, 12:00, and 18:00 UTC daily
255 (dataset ds084.6), were used to drive the CReSS model predictions. The horizontal
256 resolution of the data is $0.25^\circ \times 0.25^\circ$, and 26 of vertical levels, and the forecast fields are
257 provided every 3 h from the initial time out to a range of 192 h. The data link is also placed
258 in the “code and data availability” section.

259 To evaluate of the predictability of the D18 event using an ensemble time-lagged high-
260 resolution system and investigate the ensemble sensitivity of variables for the rainfall, 29
261 experiments were performed. The first member was initialized at 12:00 UTC on 3
262 December and the last one at 12:00 UTC on 10 December 2018. Between them, a new
263 member was initialized every 6 h and all members have a simulation length of 192 h. All
264 experiments used a single domain at 2.5 km horizontal grid spacing and a dimension in (x ,
265 y , z) of $912 \times 900 \times 60$ grid points (Table 1, cf. Fig. 2). As mentioned above, the NCEP
266 GFS was used as the IC/BCs of the CReSS model.

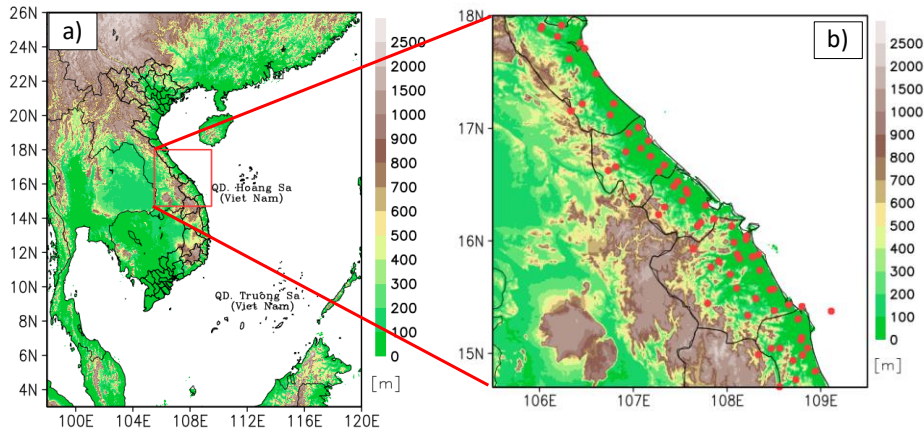


Figure 2. (a) The simulation domain of the CReSS model and topography (m, shaded) used in the study. The red box marks the study area. (b) The distribution of the observation stations (red dots) in the study area.

Table 1. The basic information of experiments.

Domain and Basic setup	
Model domain	3°–26°N; 98°–120°E
Grid dimension (x, y, z)	912 × 900 × 60
Grid spacing (x, y, z)	2.5 km × 2.5 km × 0.5 km*
Projection	Mercator
IC/BCs (including SST)	NCEP GDAS/FNL Global Gridded Analyses and Forecasts (0.25° × 0.25°, every 6 h, 26 pressure levels)

Topography (for CTRL only)	Digital elevation model by JMA at (1/120) ^o spatial resolution
Simulation length	192 h
Output frequency	1 hour
Model physical setup	
Cloud microphysics	Double-moment Bulk cold-rain scheme (six species, Lin et al., 1983; Cotton et al., 1986; Murakami, 1990, 1994; Ikawa and Saito, 1991)
PBL parameterization	1.5-order closure with prediction of turbulent kinetic energy (Deardorff, 1980; Tsuboki and Sakakibara, 2007)
Surface processes	Energy and momentum fluxes, shortwave and longwave radiation (Kondo, 1976; Louis et al., 1982; Segami et al., 1989)
Soil model	41 levels, every 5 cm deep to 2 m

* The vertical grid spacing (Δz) of CReSS is stretched (smallest at bottom) and the averaged value is given in the parentheses

2.3 Verification of model rainfall

In order to verify model-simulated rainfall, some verification methods are used, including (1) visual comparison between the model and the observation (from the 69 automated gauges over the study area), and (2) objective verification using categorical skill scores at various rainfall thresholds from the lowest at 0.05 mm up to 900 mm for three-day total. These scores are presented below along with their formulas and interpretation. To apply these scores at a given threshold, the model and observed value pairs at all verification points N (gauge sites here) are first compared and classified to construct a 2×2 contingency

table (Wilks, 2006). At any given site, if the event takes place (reaching the threshold) in both model and observation, the prediction is considered a hit (H). If the event occurs only in observation but not the model, it is a miss (M). If the event is predicted in the model but not observed, it is a false alarm (FA). Finally, if both model and observation show no event, the outcome is correct rejection (CR). After all the points are classified into the above four categories, the categorical scores can be calculated by their corresponding formula as:

$$\text{Bias Score (BS)} = (H + FA)/(H + M), \quad (1)$$

$$\text{Probability of Detection (POD)} = H/(H + M), \quad (2)$$

$$\text{False Alarms Ratio (FAR)} = FA/(H + FA), \quad (3)$$

$$\text{Threat Score (TS)} = H/(H + M + FA). \quad (4)$$

The values of TS, POD, and FAR are all ranged from 0 to 1, and the higher the better for both TS and POD, but the opposite for FAR. For BS, its possible value can vary from 0 to N and indicate overestimation (underestimation) by the model for the events if greater than (less than) unity.

2.3.1 The Similarity Skill Score

In addition to the categorical scores, the Similarity Skill Score (SSS, Wang et al., 2022) is also applied to evaluate the model rainfall results, as

$$\text{SSS} = 1 - \frac{\frac{1}{N} \sum_{i=1}^N (F_i - O_i)^2}{\frac{1}{N} \sum_{i=1}^N F_i^2 + \frac{1}{N} \sum_{i=1}^N O_i^2}, \quad (5)$$

where N is the total number of verification points as before, and F_i is the forecast rainfall amount and O_i is the observed value at the i th point among N , respectively. The SSS is a measure against the worst mean squared error (MSE) possible. The formula shows that a forecast with perfect skill has an SSS of 1, while a score of 0 means zero skill when the model rainfall does not overlap with the observation anywhere.

Note that even though Eq. (5) has the same form as the Fractions Skill Score (Roberts and Lean, 2008), the SSS is not a neighborhood method. Thus, it is suited for QPF verifications where the rainfall location is important (as in our case).

2.3.2. The ensemble spread (standard deviation)

The ensemble spread is a measure of the difference among the members about the ensemble mean, and one suitable parameter is the standard deviation (SD). In other words, the ensemble spread reflects the diversity of all possible outcomes. Hence, the ensemble spread is often applied to describe the magnitude of the forecast errors. For a well calibrated ensemble. For example, a small spread indicates high theoretical forecast accuracy (and low uncertainty), and vice versa for a large spread (Cattoën et al. 2020). Using the SD, the spread is computed by the formula below:

$$SD = \sqrt{\frac{\sum_{i=1}^n (x_i - \mu_x)^2}{n-1}}, \quad (6)$$

where x_i is the predicted value of member i for the variable x , μ_x is the ensemble mean, and n is the total number of ensemble members, respectively.

2.3.3. Ensemble Sensitivity Analysis

As mentioned above, an ensemble forecast is a set of forecasts produced by many separate forecasts typically with different initial conditions. Moreover, as we know, NWP outcomes are often sensitive to small changes in ICs and the sensitivity analysis is considered a method to improve forecasts through targeting observations. Hence, this study used the ESA method introduced by Ancell and Hakim (2007) to examine how a forecast variable responds to changes in ICs. The ensemble sensitivity is computed by the formula:

$$\frac{\partial R}{\partial x_t} = \frac{COV(R, x_t)}{VAR(x_t)}. \quad (7)$$

Here, the response function R is chosen to be the areal-mean 24-h accumulated rainfall in central Viet Nam (15.5°-16.3°N, 107.9°-108.6°E) on the rainiest day, from 12:00 UTC 9

332 to 12:00 UTC 10 December 2018. The starting time of this period, i.e., 12:00 UTC 9
333 December, is defined as t_0 . Various scalar variables are considered for x_t , at a time from 48
334 h earlier (t_{-48} , or 12:00 UTC 7 December) to t_0 at 24-h intervals. The *COV* is the covariance
335 of R and x_t , and *VAR* is the variance of x_t , respectively.

336 Since the analysis in part 1 has identified that the D18 event was caused by the combined
337 effect between the atmospheric disturbances at lower levels, such as the cold surge and
338 easterly wind, and the topography, the ESA herein has been applied to selected variables
339 at surface, near-surface, and mid-tropospheric levels to assess the sensitivity of the rainfall
340 field to ICs and its predictability. In order to facilitate the comparison among the impacts
341 of different variables, this study normalized ESA results by using the standardized anomaly
342 in the denominator of Eq. (7) and expressed them as the change in R (in mm) in response
343 to an increase in x_t by one SD in subsequent sections.

344 **3 Model results**

345 **3.1 Time-lagged 24-h QPFs by the CReSS model**

346 In this section, time-lagged forecasts targeted for the 24-h period from 12:00 UTC on 9 to
347 12:00 UTC on 10 December in the D18 event by the 2.5-km CReSS model are presented
348 and evaluated. This 24-h period is chosen because it is the rainiest day with in-situ
349 observation exceeding 600 mm at some stations (Fig. 3 OBS). Figure 3 shows 25 possible
350 scenarios of 24-h rainfall and average surface winds over the target period produced by the
351 lagged runs every 6 h, with the earliest initial time at 12:00 UTC 3 December and the latest
352 one at 12:00 UTC 9 December 2018. ~~This is true for a well calibrated ensemble, only.~~ It is
353 immediately clear that several members made a rather good 24-h QPF not only in amounts,
354 but also in rainfall location and spatial distribution. These include most members starting
355 during 8-9 December, and also an impressive member from 18:00 UTC 4 December. In
356 this latter run, a reasonably good QPF was produced at a rather long lead time, almost five
357 days (114 h) prior to the beginning of the target period. A common feature among these
358 good members is that they all captured the direction and magnitude of surface winds quite

359 well. On the other hand, most other members were less ideal in their QPFs when initialized
360 before 06:00 UTC on 7 December at lead times beyond two days (before the target period).
361 In general, they also did not predict the surface winds well enough.

362

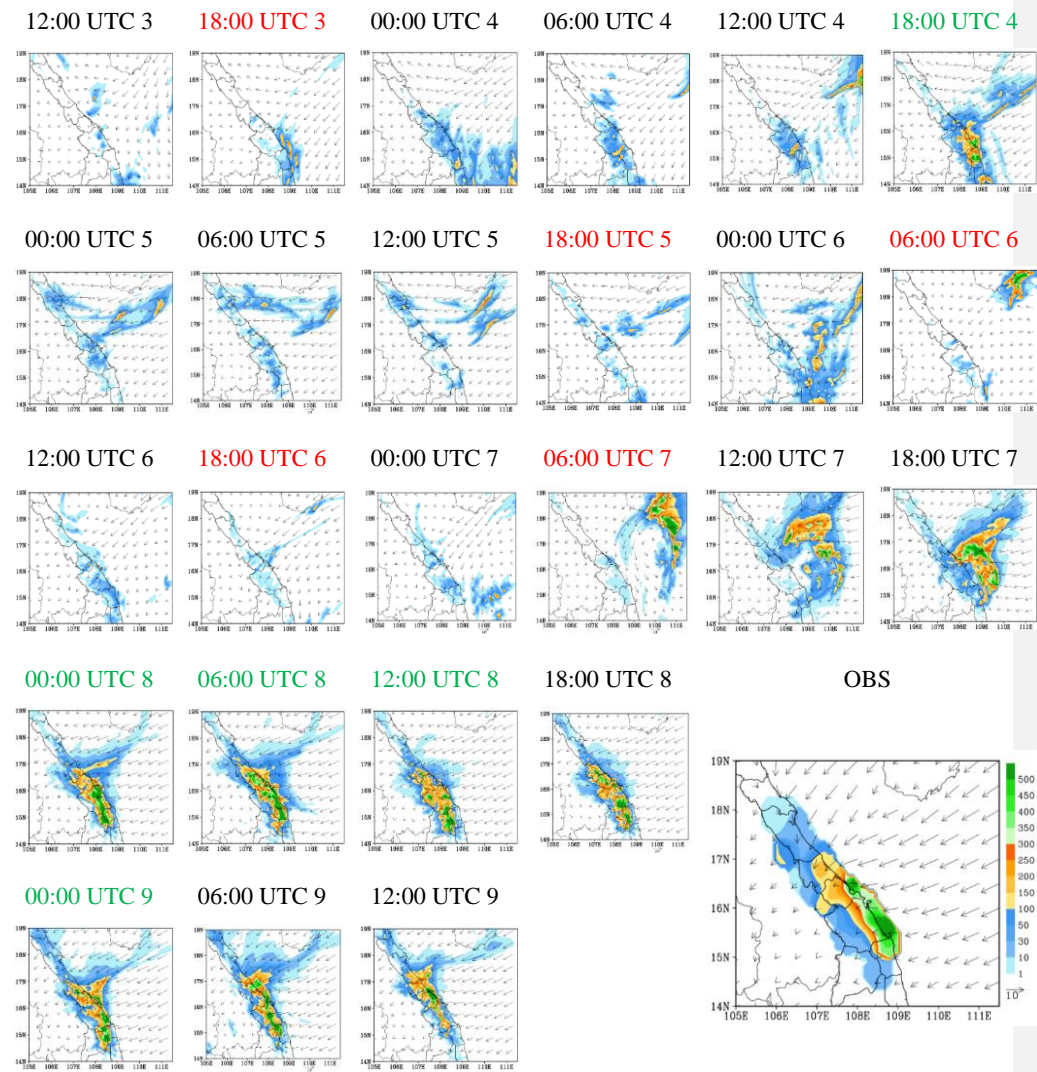


Figure 3. The predicted 24h accumulated rainfall (mm, shaded, scale on the right of panel OBS) and the mean surface horizontal wind (ms^{-1} , vector, reference length at panel OBS) on 10 December 2018 (from 12:00 UTC 9 December to 12:00 UTC 10 December 2018). The green color mark good members and the red color marks bad members. In OBS, 24h in-situ observed rainfall (mm, shaded) and the surface wind derived from ERA5 data (ms^{-1} , vector), adapted from Fig. 12f of Wang and Nguyen (2023).

Furthermore, as we know, ensemble weather forecasts are a set of forecasts from multiple members that represent the range of future weather possibilities, and the simplest way to use them is through the ensemble mean, which emphasizes the features that the members agree upon. In order to see how well the 2.5-km CReSS can predict the D18 event with the time-lagged strategy in terms possible scenarios of 24-h accumulated rainfall for 10 December, lagged runs are grouped based on their range of initial times in Fig. 4. It can be clearly seen that the rainfall predictions by the fifth four (executed between 12:00 UTC 7 and 06:00 UTC 8 December) and the sixth four members (between 12:00 UTC 8 and 06:00 UTC 9 December) are quite similar to the observation, not only in rainfall amount but also in the locations of concentrated rainfall. For other subgroups, the rainfall was much lower than the observation in their scenarios. In which, the rainfall accumulations from the third (12:00 UTC 5 to 06:00 UTC 6 December) and fourth four (12:00 UTC 6 to 06:00 UTC 7 December) members are the lowest. One relevant assessment to the outcome of these eight runs is that none of them predicted the surface wind field well enough at their ranges (beyond three days), as discussed previously. On the other hand, the mean rainfall from the second four members (12:00 UTC 4 to 06:00 UTC 5 December) is the best among all subgroups at the extended range due to a single good forecast initialized at 18:00 UTC on 4 December [cf. Fig. 3 (18:00 UTC 4)].

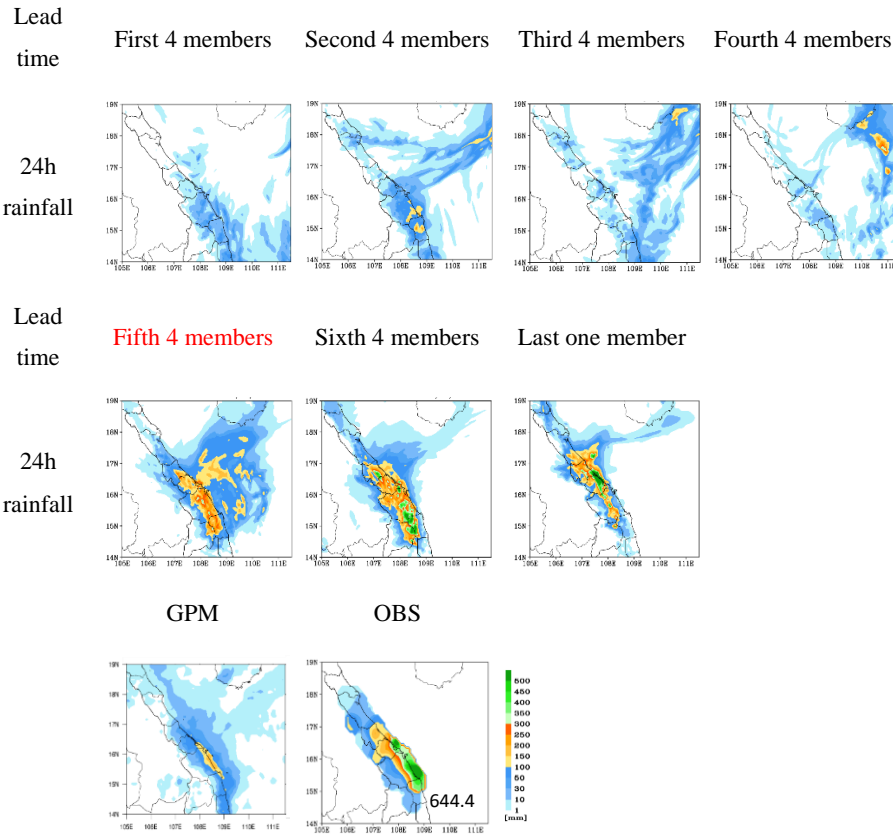


Figure 4. The predicted 24h rainfall by subgroup members, 24h accumulated rainfall by the Global Precipitation Measurement (GPM) estimate (IMERG Final Run product), 24h observed rainfall (mm, peak amount labeled at the lower-right corner) for the period of 12:00 UTC 9 December – 12:00 UTC 10 December 2018 as labelled. The same color bar (lower right) is used for all panels.

Besides the evaluation on time-lagged results using batches of successive runs (every 4 members) as presented above, this study also grouped the members using different ensemble sizes based on their behavior in order to better assess the temporal evolution of forecast uncertainty and event predictability as the lead time shortened. Particularly, the 25 members were divided into several subgroups as shown in Fig. 5, including the first eight members (those executed during 12:00 UTC 3–06:00 UTC 5 December), the middle eight members (runs between 12:00 UTC 5 and 06:00 UTC 7 December), the last nine members (12:00 UTC 7–12:00 UTC 9 December), and the last five members (12:00 UTC 8–12:00 UTC 9 December), respectively. In other words, the last five members were those executed within 24 h (1 day) prior to the beginning of the target period, and so on.

In Fig. 5, it is clear that both the ensemble means from the last five and the last nine members compare quite favorably to the observation, not only in the accumulated amount but also in spatial distribution of rainfall. This indicates that the model could produce QPFs at fairly good quality and rather consistently since the time as early as roughly 48 h prior to the commencement of the rainfall event (also Fig. 3). These two sub-groups within the short range gave much better quality in QPFs than the other sub-groups executed before them at longer lead times, including the first eight, middle eight, and all 25 members.

In terms of skill scores, for example, the mean QPF by the last five members have $TS = 0.4$, $POD = 0.8$, $BS = 1.5$, and $FAR = 0.5$ at 100 mm (per 24 h), while the last nine members give similar scores of $TS = 0.5$, $POD = 0.8$, $BS = 1.4$, and $FAR = 0.5$ (Figs. 6a-d), respectively. On the contrary, the mean QPFs from both the first and middle eight members only yield zero scores in TS , POD , and BS with no skill in FAR at 100 mm (and above), obviously due to not enough rainfall in central Viet Nam in most of their members. At 200 mm (per 24 h), similarly, the last five members ($TS = 0.2$, $POD = 0.4$, $BS = 1.4$, and $FAR = 0.7$) and the last nine members ($TS = 0.3$, $POD = 0.5$, $BS = 1.2$, and $FAR = 0.6$) again produce much better scores in QPFs, compared to no skill in all four scores in QPFs from the middle eight, first eight, and all 25 members (Figs. 6a-d). In SSS, the mean from the

last nine members exhibits the highest score (0.64), the middle eight members have the lowest score (0.04), and the mean from all 25 members is 0.43 (Fig. 6e).

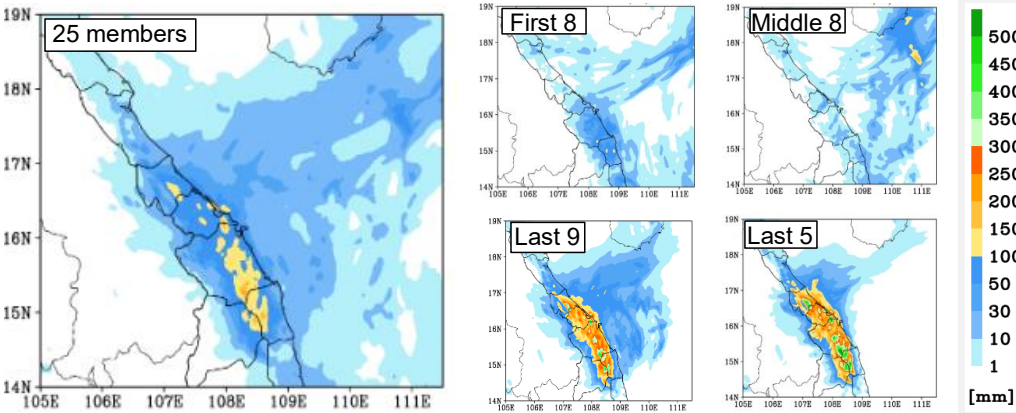
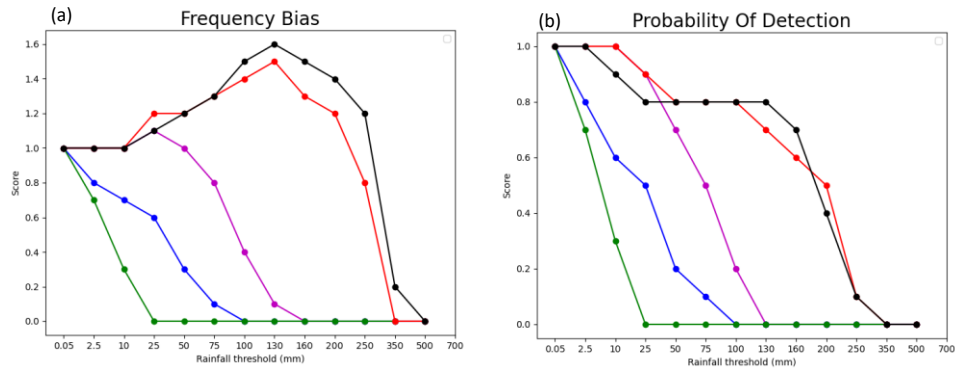


Figure 5. Ensemble mean rainfall (shaded, scale on the right) from all 25 time-lagged members, executed every 6 h from 12:00 UTC 3 December to 12:00 UTC 9 December, for the 24h period from 12:00 UTC 9 December to 12:00 UTC 10 December.



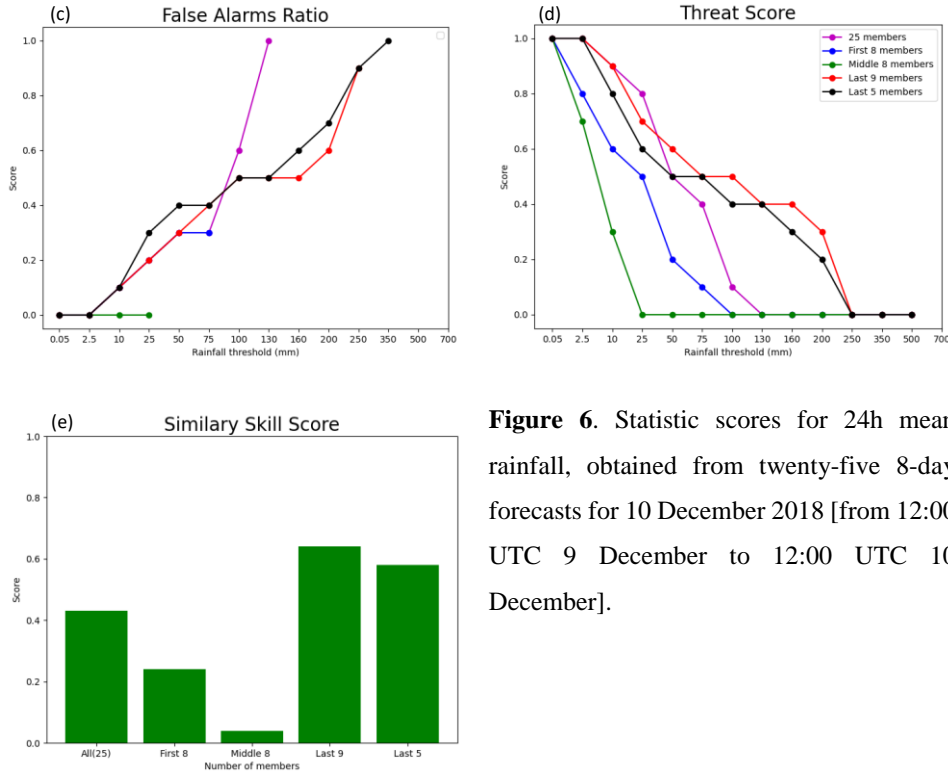


Figure 6. Statistic scores for 24h mean rainfall, obtained from twenty-five 8-day forecasts for 10 December 2018 [from 12:00 UTC 9 December to 12:00 UTC 10 December].

432

433 However, as indicated by the SD, the spreads in rainfall scenarios in both ensembles from

434 the last five and nine members are quite large (Fig. 7). Thus, while the lagged members

435 can produce a wide range of possible rainfall scenarios for the D18 event, which is the

436 main purpose of an ensemble as reviewed in Section 1, the members often cannot agree on

437 the precise locations of heavy rainfall. Given the small scale of local convection during the

438 event, this result is perhaps anticipated. On the other hand, the maxima in spread are >160

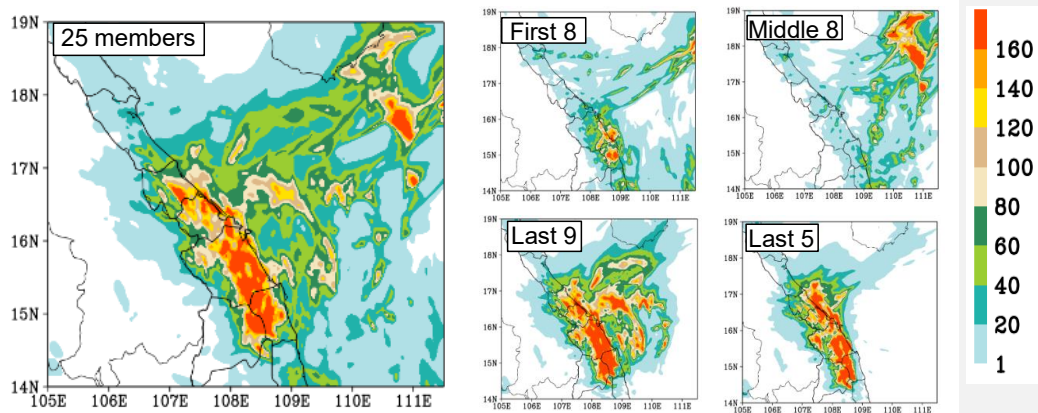
439 mm in Fig. 7 among the last nine members, perhaps quite reasonable in magnitude

440 compared to the peak amounts of about 400 mm in the ensemble mean. In any case, Figs.

441 6 and 7 indicate that the predictability of the D18 event changed considerably with time,

442 and the 2.5-km CReSS has a good skill in QPFs inside the short range (≤ 72 h). However,
 443 it remains difficult to predict the event successfully at longer lead times.

444



445

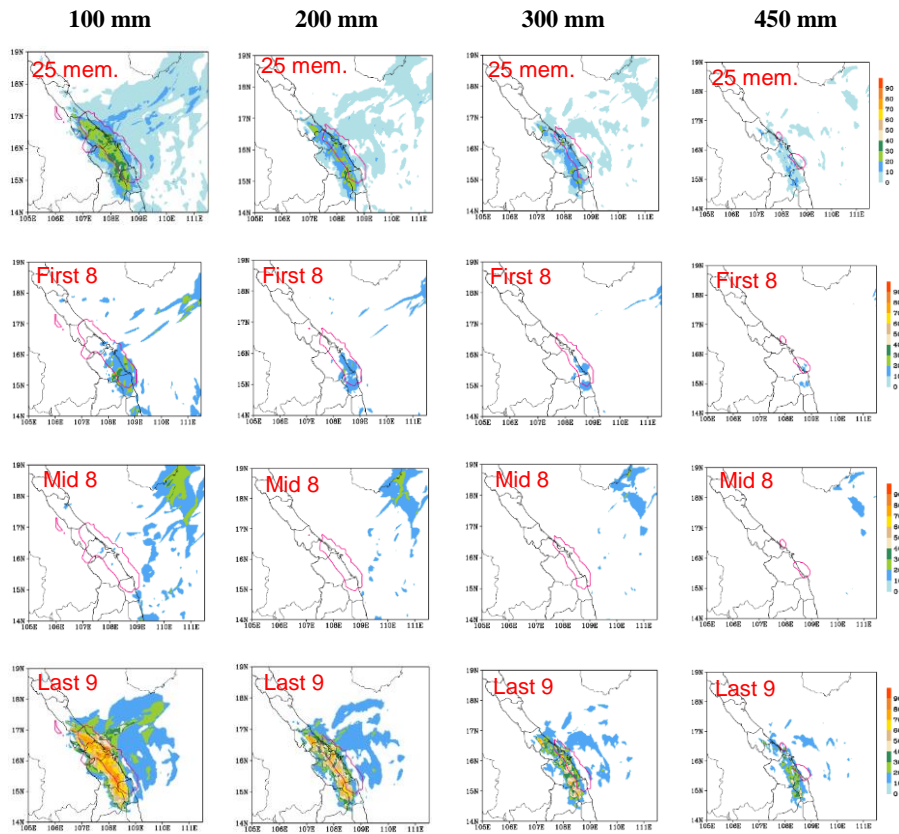
446 **Figure 7.** The spread (shaded, scale on the right) from all 25 time-lagged members,
 447 executed every 6 h from 12:00 UTC 3 December to 12:00 UTC 9 December, for the 24h
 448 period from 12:00 UTC 9 December to 12:00 UTC 10 December.

449

450 The probability information derived from the sub-ensemble groups at four different rainfall
 451 thresholds from 100 to 450 mm is shown in Fig. 8, in which the increase in heavy-rainfall
 452 probability in central Viet Nam and thus the predictability of the event with time is also
 453 evident. From the first eight members executed at the longest range (≥ 102 h prior to rainfall
 454 accumulation), there is only a 10-25% chance in parts of central Viet Nam to receive at
 455 least 100 mm of rainfall for 10 December (from 12:00 UTC 9 to 12:00 UTC 10 December).
 456 The probability is even lower from the middle eight members (run between 54-96 h prior
 457 to target period), as their SSS is the lowest among all sub-ensemble groups and only a
 458 couple of the runs could reach 100 mm anywhere inland in central Viet Nam. As the lead

459 time shortens to inside the short range, the probabilities to have ≥ 100 mm of rainfall
 460 increase dramatically, to roughly 70-80 % in the last nine members and further to over 80-
 461 90% in the last five members. Due to the contribution from later members, about 20-40%
 462 of all 25 members can reach 100 mm inland. Toward higher thresholds, the probabilities
 463 decrease in Fig. 8 as expected, so do the areal sizes actually reaching those thresholds (pink
 464 contours). At the highest value of 450 mm, the ensembles in general show less than about
 465 20%-30% chance for its occurrence from the last five and last nine members, respectively,
 466 and the high probability areas are also slightly more inland than the observed one.

467



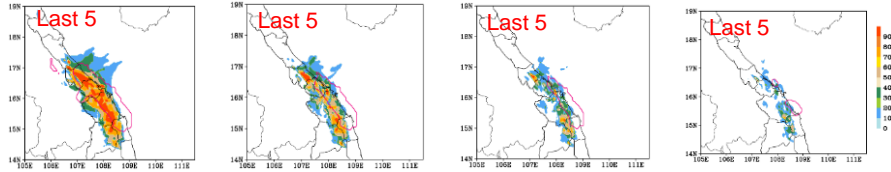


Figure 8. Probability distribution (%) (shaded, scale on the right) from all 25 time-lagged members, executed every 6 h from 12:00 UTC 3 December to 12:00 UTC 9 December, reaching thresholds of 100, 200, 300, and 450 mm, for the 24h period from 12:00 UTC 9 December to 12:00 UTC 10 December. The observed areas at the same thresholds are depicted by the pink contours. For each picture, red labeled at the top-left corner show the number of members grouped to calculate the probability distribution.

3.2 Ensemble-based sensitivity analysis

The results in Section 3.1 above reveal that the CReSS model with a horizontal grid size of 2.5 km predicted good QPFs for the rainiest day of the event and performed better than those reviewed in Section 1. Therefore, relying on this good performance, the ESA is carried out in this subsection.

Firstly, five good members (those with initial times at 18:00 UTC on 4, 00:00, 06:00, and 12:00 UTC on 8, and 00:00 UTC on 9 December) and five bad ones (those ran at 18:00 UTC on 3, 18:00 UTC on 5, 06:00 and 18:00 UTC on 6, and 06:00 UTC on 7 December) are chosen and by using their differences (good minus bad members), Fig. 9 shows that the main reason for the significantly different forecast outcomes lies in differences in the input datasets (i.e., IC/BCs). Specifically, the surface easterly winds were much stronger and the relative humidity much higher surrounding central Viet Nam and its upstream areas in the GFS forecast data valid at 12:00 UTC on 9 December (used as BCs in CReSS runs) in the good members than in the bad ones (Fig. 9a). Subsequently, the good CReSS members produced much more rainfall in central Viet Nam (Fig. 9b). These factors were also identified as crucial for the extreme rainfall in the D18 event in Part 1.

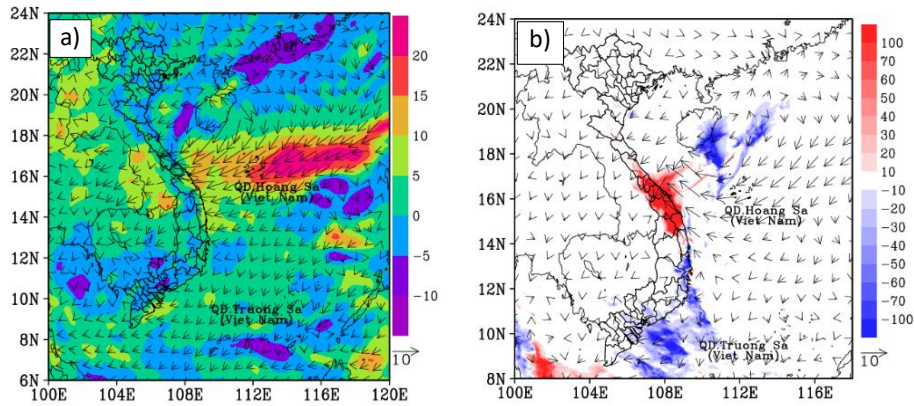


Figure 9. The difference in (a) input data (boundary conditions) and (b) CReSS output between averaged 5 good members (members ran at 18:00 UTC 4, 00:00 UTC 8, 06:00 UTC 8, 12:00 UTC 8, 00:00 UTC 9) and 5 bad members (members ran at 18:00 UTC 3, 18:00 UTC 5, 06:00 UTC 6, 18:00 UTC 6, 06:00 UTC 7). For input data, relative humidity (% , shaded) and surface wind (ms^{-1} , vector) at 12:00 UTC December 9 2018. For CReSS output, 24-h accumulated rainfall (mm, shaded) and surface wind (ms^{-1} , vector).

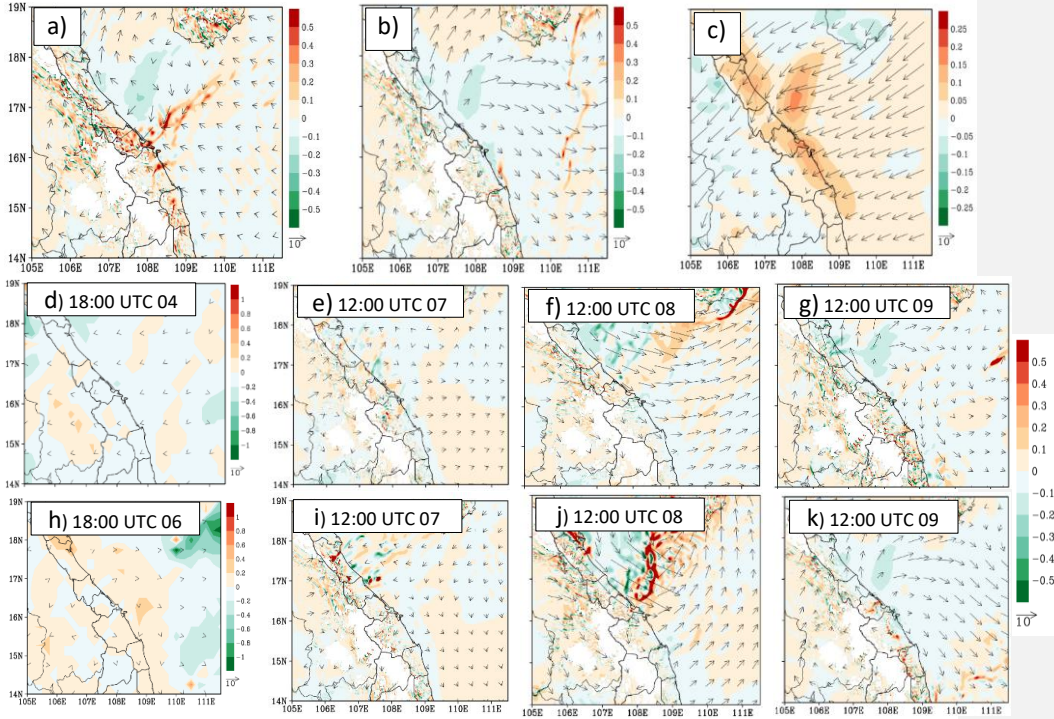
Meanwhile, Fig. 10 shows the difference in the evolution of synoptic-scale patterns (features) zoomed into the study area. To be more specific, Fig. 10a depicts the difference (CReSS output minus NCEP FNL analysis) in the horizontal wind and vertical velocity between the averages of the 5 good members and the NCEP FNL analysis at 925 hPa at 12:00 UTC 9, and it is small although each member was initialized at a different lead time. It implies that these members captured well the evolution of weather patterns of this event. Additionally, the model vertical velocity is seen to be stronger than the NCEP FNL data. Therefore, these members produced the rainfall closer to the observation with the presence of complex terrain in the study area. On the contrary, bad members did not capture the evolution of weather patterns well enough (Fig. 10b), and they could not produce good QPFs as a result.

508 Furthermore, Fig. 10d indicates very small differences in the IC of the member that was
509 initialized at 18:00 UTC 4 to the FNL analysis (thus suggesting smaller errors), especially
510 over the study area. From this initial data, the evolution of weather patterns in this CReSS
511 run also agreed well with the analyses during the first three days (not shown), and the
512 differences remained relatively small even at 12:00 UTC 9, at a lead time of roughly 5 days
513 (Figs. 10e,f,g). Compare to this, a bad member initialized at 18:00 UTC 6 (at a shorter lead
514 time by 2 days) exhibited somewhat larger differences in the initial state in relation to the
515 NCEP FNL analysis (Fig. 10h). This difference then led to larger and more evident
516 differences in weather patterns, as seen in Figs. 10 i, j, k by this particular member that
517 performed worse in QPFs (member ran at 18 UTC 06). The results here not only indicate
518 that it is still possible to have good rainfall forecasts at a lead time up to 5 days, but also
519 show some predictability by a cloud-resolving model at such long lead times.

520

521

522



523

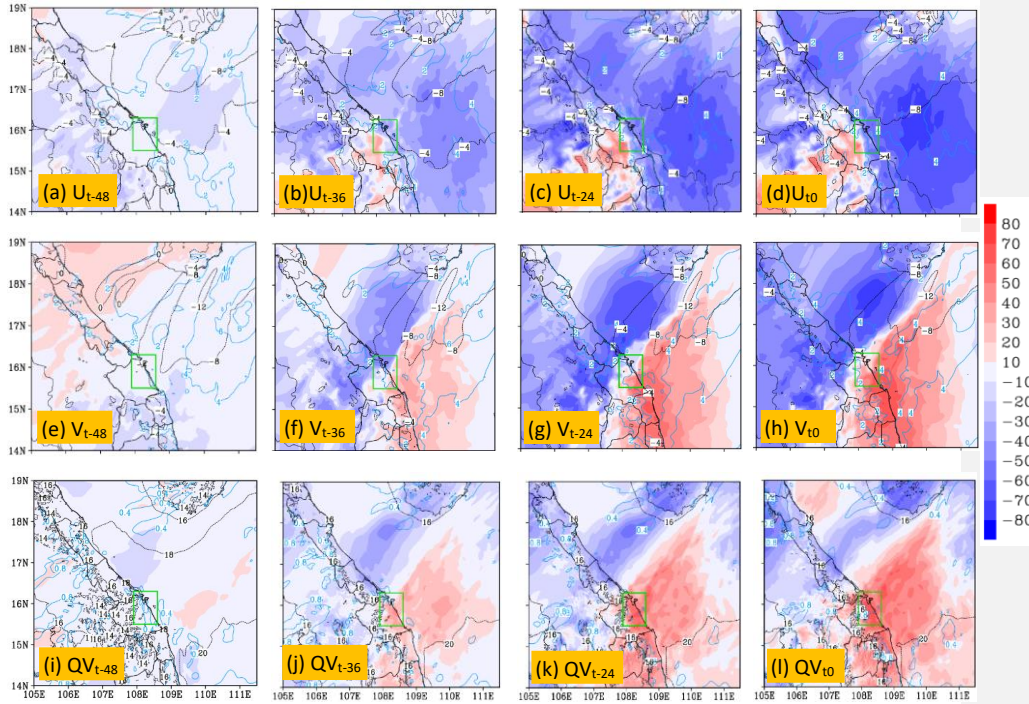
524 **Figure 10.** The difference in the horizontal wind (ms^{-1} , vector, reference length at the low-
525 right corner of the panel), and vertical velocity (ms^{-1} , shaded, the reference color scale is
526 on the right of panel) between (a) averaged 5 good members and (b) averaged 5 bad
527 members and the NCEP FNL analysis data at 925 hPa and at 12 UTC 09. (c) The NCEP
528 FNL analysis horizontal wind (ms^{-1} , vector, reference length at the low-right corner of the
529 panel) and vertical velocity (ms^{-1} , shaded) at 925 mb and at 12 UTC 09. (d) The difference
530 in the horizontal wind (ms^{-1} , vector, reference length at the low-right corner of the panel),
531 and relative humidity (% , shaded, the reference color scale is on the right of panel) between
532 the initial data of a good member at a longer lead time (at 1800 UTC 4 Dec) and the NCEP
533 FNL analysis data at 925 hPa. (e), (f), and (g) present the difference in the evolution of
534 weather features with time by this good member. (h) as in (d) but for a bad member
535 (member ran at 1800 UTC 6 Dec). (i), (j) and (k) as in (e), (f), and (g), respectively, but for

536 mentioned bad member. Compared variables are horizontal wind at 925 hPa (ms^{-1} , vector,
537 reference length at the low-right corner of the panel) and vertical velocity (ms^{-1} , shaded,
538 the reference color scale is on the right of panel). The NCEP FNL analysis horizontal wind
539 (ms^{-1} , vector, reference length at the low-right corner of the panel) and vertical velocity
540 (ms^{-1} , shaded) at 925 mb.

541 Additionally, the above results also reaffirm that very small differences in the initial data
542 can lead to a vastly different outcome, especially as the forecast range increases, in extreme
543 rainfall events (such as the D18 event) that involve highly nonlinear deep convection. As
544 pointed out in Part 1, the low-level wind convergence led to moisture convergence and
545 these conditions played a crucial role in the D18 event. The southward movement of the
546 low-level wind convergence also dictated the movement of the convective rainband during
547 the event. Therefore, the ESA was applied on relevant variables, including the horizontal
548 wind and mixing ratio of water vapor. The quantitative results are shown in Figs. 11-13
549 and presented below.

550 Figure 11 shows the sensitivity of mean 24-h total rainfall inside the green box in central
551 Viet Nam (R) to zonal (u) and meridional (v) wind components and water vapor mixing
552 ratio (q_v) at the surface, with the ensemble mean also plotted. It is clear that the sensitivity
553 of rainfall to these variables is lower at longer forecast ranges and becomes higher as the
554 lead time shortens. Specifically, from two days before (t_{-48}) to the starting time of the
555 accumulation period (t_0), the sensitivity of rainfall to u -wind over the SCS and along the
556 coast of central Viet Nam turned more negative, indicating heavier rainfall associated with
557 stronger easterly winds ($u < 0$) near the surface, especially in areas immediately upstream
558 toward t_0 (Figs. 11a-d). The rainfall's sensitivity to v -wind leading to t_0 , on the other hand,
559 exhibited a dipole structure in pattern, with negative values to the north-northwest and
560 positive values to the south-southeast across central Viet Nam and the upstream ocean
561 (Figs. 11e-h). This structure indicates a stronger confluence in northeasterly winds over the
562 region in rainier members, consistent with the results in Part 1. In Figs. 11e-h, the increase
563 in v -wind just south of central Viet Nam is particularly evident, from -10 mm per SD (SD

564 $= 2 \text{ ms}^{-1}$) at t_{-48} to over $+70 \text{ mm}$ per SD ($\text{SD} = 2\text{--}4 \text{ ms}^{-1}$) at t_0 . Thus, the precipitation amount
 565 over central Viet Nam in the D18 event is highly sensitive to the strength and confluence
 566 of northeasterly winds near the surface in short-range forecasts. Similarly, the rainfall was
 567 also highly sensitive to the water vapor amount and its flux convergence (Figs. 11i-l).



568 **Figure 11.** The sensitivity (mm, per SD, color, scale on the right) of areal-mean 24h
 569 accumulated rainfall in central Viet Nam starting from t_0 (i.e., R, averaging area depicted
 570 in green box) to surface wind components (ms^{-1} , shaded) and the ensemble mean (contours,
 571 every 4 ms^{-1}) and to surface water vapor mixing ratio (r , g kg^{-1}) and its ensemble mean
 572 (contours, every 0.06 g kg^{-1}) at different times at 24h intervals from (a) t_{-48} to (f) t_0 . The
 573 time of t_0 is 12:00 UTC 9 December 2018. In which, (a), (b), (c), (d) for the zonal wind
 574 component. (e), (f), (g), (h) for the meridional wind component, and (i), (j), (k), (l) for

575 surface water vapor mixing ratio. The standard deviation is exhibited by the medium blue
 576 contours.

577 Slightly higher up at 1476 m (near 850 hPa), where easterly flow prevailed during the D18
 578 event (see Fig. 3b in Part 1), the sensitivity of rainfall to u and v winds exhibits similar
 579 spatial patterns (Figs. 12a-h) to those at the surface (Figs. 11a-h), with stronger easterly
 580 winds and larger confluence in association with heavier rainfall. Similarly, the rainfall in
 581 central Viet Nam is still highly sensitive to mixing ratio at this level, both locally and over
 582 the surrounding area scale (Figs. 12i-l), again especially at shorter lead times. At the local
 583 scale, this positive correlation presumably is linked to upward transport of moisture, as the
 584 ascending motion in convective clouds could become larger at this level (and also more
 585 vigorous in rainier members).

586

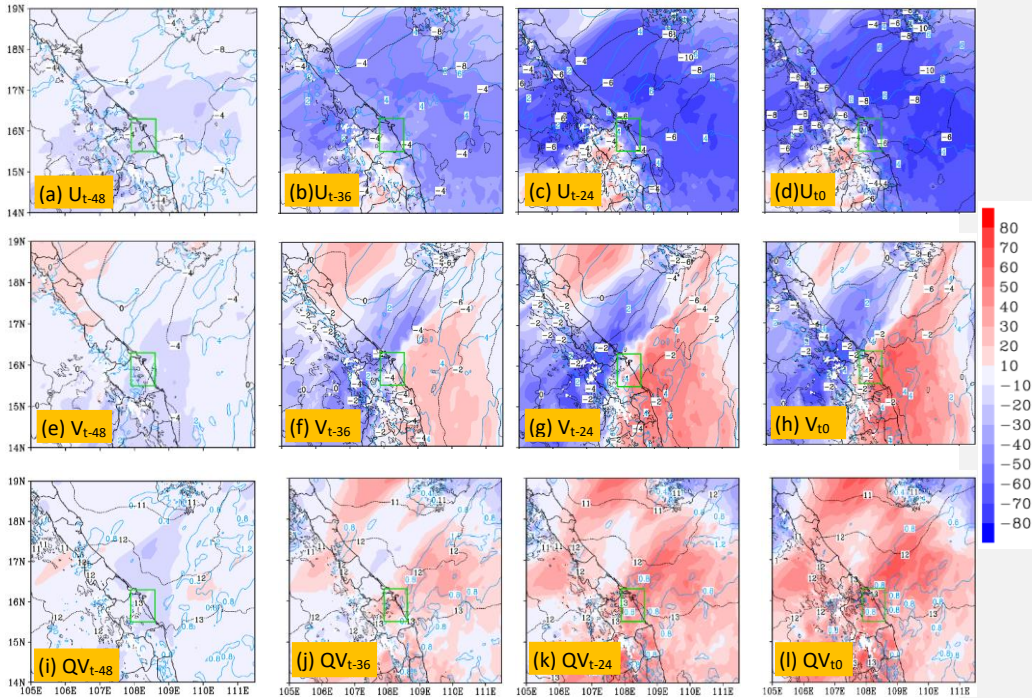


Figure 12. The sensitivity (mm, per SD, color, scale on the right) of 24h accumulated rainfall in central Viet Nam starting from t_0 (i.e., R, averaging area depicted in green box) to the wind components (ms^{-1} , shaded) and the ensemble mean (contours, every 2 ms^{-1}) and to water vapor mixing ratio (r , g kg^{-1}) and its ensemble mean (contours, every 0.4 g kg^{-1}) at attitude of 1476 m and at different times at 24h intervals from (a) t_{-48} to (f) t_0 . The time of t_0 is 12:00 UTC 9 December 2018. In which, (a), (b), (c), (d) for the zonal wind component. (e), (f), (g), (h) for the meridional wind component, and (i), (j), (k), (l) for water vapor mixing ratio. The standard deviation is exhibited by the medium blue contours.

At the upper level of 5424 m (near 500 hPa), it is seen that from t_{-48} to t_0 , dipole structures developed in the sensitivity patterns of rainfall to both u and v winds (Figs. 13a-h). To u winds, positive sensitivity up to about +70 mm per SD ($\text{SD} = 2\text{-}4 \text{ ms}^{-1}$ depending on t) existed to the south, with negative values up to -70 mm per SD ($\text{SD} = 2\text{-}4 \text{ ms}^{-1}$) to the north of central Viet Nam. Meanwhile, positive sensitivity to v -wind appeared to the north and east with negative sensitivity to the south and west of the rainfall area. As the prevailing winds at 500 hPa were southeasterlies over southern Viet Nam and southwesterlies over northern Viet Nam during the D18 event (thus with anticyclonic curvature, see Fig. 3c in Part 1), the above sensitivity patterns, already apparent at t_{-24} (Figs. 13c,g), corresponded to stronger diffluence/divergence and a weaker anticyclone aloft to favor more rainfall. To q_v , positive sensitivity signals up to +70 mm per SD ($\text{SD} = 1.2 \text{ g kg}^{-1}$) also appeared over the rainfall area at t_{-24} and t_0 (Figs. 13i-l), and the reason is similar to that near 850 hPa in Fig. 12. Overall, the ESA performed in this study indicated clearly that the synoptic pattern that caused the D18 event already developed at times more than 24 h earlier, and this explains why, with a high enough resolution and cloud-resolving capability, the CReSS forecasts could better predict and improve the QPFs inside the short range as shown in Section 3.

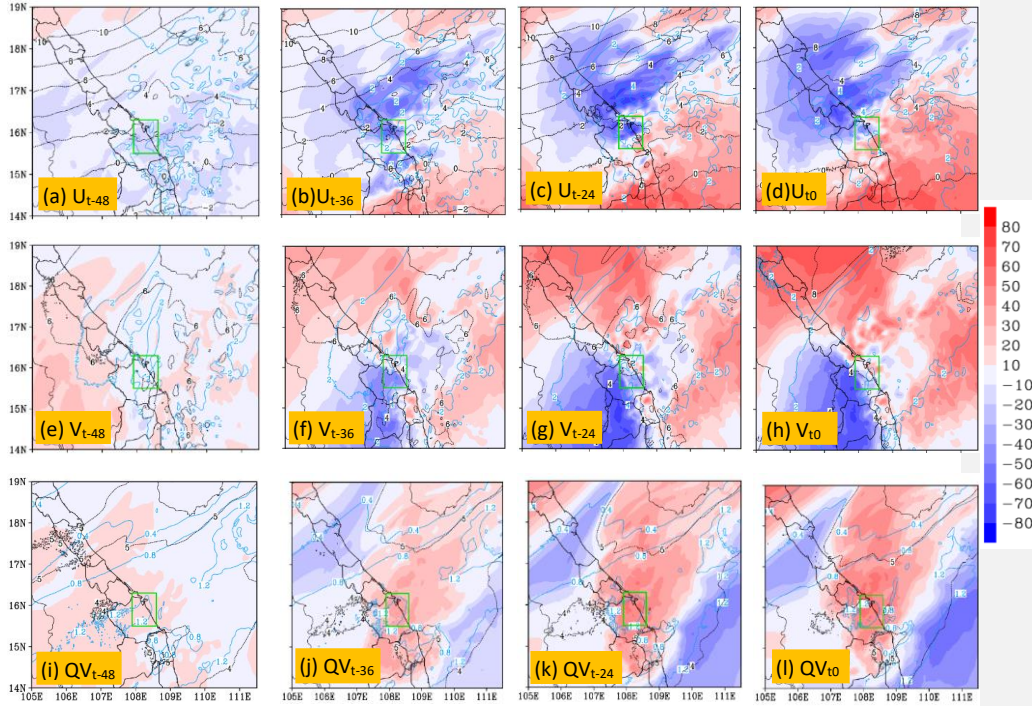


Figure 13. The sensitivity (mm, per SD, color, scale on the right) of 24h accumulated rainfall in central Viet Nam starting from t_0 (i.e., R, averaging area depicted in green box) to the wind components (ms^{-1} , shaded) and the ensemble mean (contours, every 2 ms^{-1}) and to water vapor mixing ratio (r , g kg^{-1}) and its ensemble mean (contours, every 0.4 g kg^{-1}) at attitude of 5424 m and at different times at 24h intervals from (a) t_{-48} to (f) t_0 . The time of t_0 is 12:00 UTC 9 December 2018. In which, (a), (b), (c), (d) for the zonal wind component. (e), (f), (g), (h) for the meridional wind component, and (i), (j), (k), (l) for water vapor mixing ratio. The standard deviation is exhibited by the medium blue contours.

4 Conclusion

As high resolution is required in numerical models to predict heavy rainfall more successfully, the present work utilizes a time-lagged high-resolution ensemble forecast

624 system and evaluates how well the D18 event (during 9-12 December 2018) in central Viet
625 Nam can be predicted in advance before its occurrence. Using the CReSS model with a
626 grid size of 2.5 km (912×900 in dimension with 60 vertical levels), ensemble forecasts
627 were produced with a total of 29 time-lagged runs at 6-h intervals, each out to a forecast
628 range of 192 h (eight days). Based on the goals raised from the analysis in Part 1, the key
629 findings of this Part 2 study are summarized as follows:

630 The first goal of this study is regarding the scientific hypotheses that at a higher resolution,
631 the cloud-resolving time-lagged ensemble can improve the QPFs of the D18 event at the
632 short range, and may also be able to extend the lead time of decent QPFs beyond the short
633 range. Our evaluation results confirm that this strategy using the CReSS model can
634 effectively improve the QPFs of this event at the short range. Furthermore, the results also
635 demonstrate that a decent QPF for 10 December (the rainiest day) can be made at a longer
636 lead time (initialized at 1800 UTC 4 December), when good initial conditions are provided.

637 About the second goal, our investigation in predictability indicates that the 2.5-km system
638 predicted the rainfall fields on 10 December during the event fairly well, including both
639 the amount and spatial distribution, within the short range at lead times of day 1, 2, and 3.
640 More specifically, the SSS of QPFs at these three ranges are about 0.4, 0.6, and 0.7,
641 respectively, with fairly consistent results among successive runs that indicate a reasonable
642 predictability, despite some spread and disagreement on the precise locations of heavy
643 rainfall. The above good results are due to the model's capability to better predict the
644 conditions in the lower troposphere such as the wind fields.

645 At lead times longer than three days, however, the predictability of the event is lowered
646 due to a higher level of forecast uncertainty, and the quality of QPFs drops with significant
647 under-prediction. Nevertheless, good QPFs are still possible occasionally. At lead time
648 beyond six days, it is challenging to achieve a good QPF at thresholds greater than 100 mm
649 even with a high-resolution model. This is presumably linked to the rapid evolution of
650 atmospheric conditions during such an extreme event surrounding Viet Nam in a tropical
651 environment. In the present study, a CRM is applied to forecast extreme rainfall in central

652 Viet Nam for the first time. Although still with certain limitations, our results do indicate
653 hope to predict such events successfully beforehand, at least within the short range.
654 Therefore, based on the present work, more studies on the predictability of extreme rainfall
655 in Viet Nam are recommended in the near future.

656 Regarding the third and final goal, ESA results show that the rainfall is most sensitive to
657 the wind conditions in the lower troposphere leading to the event, with more rain associated
658 with stronger northeasterly to easterly winds and their confluence over central Viet Nam
659 (and the upstream region). Similarly, the rainfall also shows strong sensitivity to the
660 moisture amount, not only at the surface but also further aloft at the upper levels. Besides,
661 ESA also indicates that the synoptic pattern that caused the D18 event already developed
662 at timing earlier in the past. Furthermore, in the ESA, the finer-scale features (convection)
663 are also seen to link to synoptic conditions in their background, implying that it is
664 meaningful to apply ESA to control the perturbations in initial fields.

665 The key findings in this study underscore that both practical predictability and ESA are
666 intertwined, influencing the design and evaluation of ensemble forecast systems, and
667 potentially applicable to other extreme rainfall events in the same season in Vietnam.

668

669 *Acknowledgements:* This study was supported by the project “*Research on the application*
670 *of the Cloud-resolving model integrated with the regional numerical model to a 6-hour*
671 *accumulated quantitative precipitation forecast with 24-48 hours lead time for Mid-*
672 *Central Viet Nam*”, which is funded by the Ministry of Natural Resources and Environment
673 (MONRE) under grant no. TNMT.2023.06.07, and also by the National Science and
674 Technology Council (NSTC) of Taiwan under grants MOST 111-2625-M-003-001, NSTC
675 112-2625-M-003-001, NSTC 113-2625-M-003-001, and NSTC 113-2111-M-003-001.

676 *Code and data availability.* The CReSS model used in this study and its user’s guide are
677 available at the model website at [http://www.rain.hyarc.nagoya-](http://www.rain.hyarc.nagoya-u.ac.jp/~tsuboki/cress_html/src_cress/CReSS2223_users_guide_eng.pdf)
678 [u.ac.jp/~tsuboki/cress_html/src_cress/CReSS2223_users_guide_eng.pdf](http://www.rain.hyarc.nagoya-u.ac.jp/~tsuboki/cress_html/src_cress/CReSS2223_users_guide_eng.pdf) (last access: 6

679 July 2023; Tsuboki and Sakakibara, 2007). The TIGGE data and its information are
680 available at <https://confluence.ecmwf.int/display/TIGGE/TIGGE+archive>. The NCEP
681 GFS dataset and its description are available at <https://rda.ucar.edu/datasets/ds084.1/>. The
682 NCEP FNL operational global gridded analysis data and its information is available at
683 <https://rda.ucar.edu/datasets/d083003/#>.

684 *Author contributions.* **Duc Van Nguyen** prepared datasets, executed the model
685 experiments, performed the analysis, and prepared the first draft of the manuscript. **Chung-**
686 **Chieh Wang** also prepared the first draft and provided the funding, guidance and
687 suggestions during the study, and they participated in the revision of the manuscript. **Kien**
688 **Ba Truong** provided the funding and participated revising of the manuscript. **Thang Van**
689 **Vu, Pham Thi Thanh Nga, and Pi-Yu Chuang** also participated in the revision of the
690 manuscript.

691 *Competing interests.* The authors declare that they have no conflict of interest.

692 References

693 Ancell, and Hakim, G. J.: Comparing adjoint- and ensemble sensitivity analysis with
694 applications to observation targeting. Mon. Wea. Rev., 135, 4117–4134,
695 doi:10.1175/2007MWR1904.1, 2007.

696 Cotton, W. R., Tripoli, G. J., Rauber, R. M., and Mulvihill, E. A.: Numerical simulation of
697 the effects of varying ice crystal nucleation rates and aggregation processes on
698 orographic snowfall. J. Appl. Meteorol. Clim., 25, 1658–1680, 1986.

699 Coleman, A. A., and Ancell, B. C.: Toward the improvement of high-impact probabilistic
700 forecasts with a sensitivity-based convective-scale ensemble subsetting
701 technique. Mon. Wea. Rev., 148, 4995–5014, [https://doi.org/10.1175/MWRD-20-](https://doi.org/10.1175/MWRD-20-0043.1)
702 [0043.1](https://doi.org/10.1175/MWRD-20-0043.1), 2020.

703 [Cattoën, C., Robertson, D. E., Bennett, J. C., Wang, Q. J., and Carey-Smith, T. K.:](#)

Formatted: English (United States)

704 Calibrating Hourly Precipitation Forecasts with Daily Observations. J. Hydrometeorol., 21,
705 1655-1673, <https://doi.org/10.1175/JHM-D-19-0246.1>, 2020.

706 Deardorff, J. W.: Stratocumulus-capped mixed layers derived from a three-dimensional
707 model. Bound.-Lay. Meteorol., 18, 495–527, 1980.

708 Hu, C.-C., and Wu, C.-C.: Ensemble sensitivity analysis of tropical cyclone intensification
709 rate during the development stage. J. Atmos. Sci., 77, 3387–3405,
710 <https://doi.org/10.1175/JAS-D-19-0196.1>, 2020.

711 Hoa, V. V.: Comparative study skills rain forecast the middle part and central highland of
712 several global models (In Viet Nameese). Viet Nam journal of Hydrometeorology. V.
713 667 No. 07 (2016), 2016.

714 Hohenegger, C., and Schär, C.: Predictability and error growth dynamics in cloud-
715 resolving models. J. Atmos. Sci., 64, 4467–4478,
716 <https://doi.org/10.1175/2007JAS2143.1>, 2007.

717 Huffman, G. J., Bolvin, D. T., Braithwaite, D., Hsu, K., Joyce, R., Kidd, C., Nelkin, E.J.,
718 Sorooshian, S., Tan, J., Xie, P.: Algorithm Theoretical Basis Document (ATBD)
719 Version 06: NASA Global Precipitation Measurement (GPM) Integrated Multi-
720 Satellite Retrievals for GPM (IMERG). NASA/GSFC, Greenbelt, MD, USA,
721 [https://gpm.nasa.gov/sites/default/files/2020-](https://gpm.nasa.gov/sites/default/files/2020-05/IMERG_ATBD_V06.3.pdf)
722 [05/IMERG_ATBD_V06.3.pdf](https://gpm.nasa.gov/sites/default/files/2020-05/IMERG_ATBD_V06.3.pdf)[https://gpm.nasa.gov/sites/default/files/2020-](https://gpm.nasa.gov/sites/default/files/2020-05/IMERG_ATBD_V06.3.pdf)
723 [05/IMERG_ATBD_V06.3.pdf](https://gpm.nasa.gov/sites/default/files/2020-05/IMERG_ATBD_V06.3.pdf), 2020.

724 Ikawa, M. and Saito, K.: Description of a non-hydrostatic model developed at the Forecast
725 Research Department of the MRI, MRI Technical report 28, Japan Meteorological
726 Agency, Tsukuba, Japan, ISSN: 0386-4049, 1991.

727 Kerr, C. A., Stensrud, D. J. and Wang, X.: Diagnosing convective dependencies on near-
728 storm environments using ensemble sensitivity analyses. Mon. Wea. Rev., 147, 495–
729 517, <https://doi.org/10.1175/MWRD-18-0140.1>, 2019.

Formatted: German (Germany)

Formatted: German (Germany)

730 Kondo, J.: Heat balance of the China Sea during the air mass transformation experiment.
731 J. Meteorol. Soc. Jpn., 54, 382–398, https://doi.org/10.2151/jmsj1965.54.6_382, 1976.

732 Leith, C. E.: Theoretical skill of Monte Carlo forecasts. Mon. Wea. Rev., 102, 409–
733 418, 1974.

734 Lin, Y.-L., Farley, R. D., and Orville, H. D.: Bulk parameterization of the snow field in a
735 cloud model. J. Appl. Meteorol. Clim., 22, 1065–1092, 1983.

736 Louis, J. F., Tiedtke, M., and Geleyn, J. F.: A short history of the operational PBL
737 parameterization at ECMWF, in: Proceedings of Workshop on Planetary Boundary
738 Layer Parameterization, 25– 27 November 1981, Shinfield Park, Reading, UK, 59–79,
739 1982.

740 Lorenz, E.N.: The predictability of a flow which possesses many scales of motion. Tellus,
741 21, 289–307. <https://doi.org/10.3402/tellusa.v21i3.10086>, 1969.

742 Lorenz, E.N.: Atmospheric predictability as revealed by naturally occurring analogues. J.
743 Atmos. Sci., 26, 636–646, 1969.

744 Murphy, J. M.: The impact of ensemble forecasts on predictability. Quart. J. Roy.
745 Meteor. Soc., 114, 463–493, 1988.

746 Murakami, M.: Numerical modeling of dynamical and microphysical evolution of an
747 isolated convective cloud – the 19 July 1981 CCOPE cloud. J. Meteorol. Soc. Jpn., 68,
748 107–128, 1990.

749 Murakami, M., Clark, T. L., and Hall, W. D.: Numerical simulations of convective snow
750 clouds over the Sea of Japan: Two dimensional simulation of mixed layer development
751 and convective snow cloud formation. J. Meteorol. Soc. Jpn. 72, 43–62, 1994.

752 Melhauser, C., and Zhang, F.: Practical and intrinsic predictability of severe and convective
753 weather at the mesoscales. J. Atmos. Sci., 69, 3350–3371, doi:10.1175/JAS-D-11-
754 0315.1, 2012.

755 Nhu, D. H., Anh, N. X., Phong, N. B., Quang, N. D., and Hiep, V. N.: The role of
 756 orographic effects on occurrence of the heavy rainfall event over central Viet Nam in
 757 November 1999. *Journal of Marine Science and Technology*. V. 17, No. 4B(2017), 31-
 758 36, 2017.

759 Nielsen, E. R. and Schumacher, R. S.: Using convection-allowing ensembles to understand
 760 the predictability of an extreme rainfall event. *Monthly Weather Review*, 144, 3651–
 761 3676, 2016.

762 Roberts, N. M. and Lean, H. W.: Scale-Selective Verification of Rainfall Accumulations
 763 from High-Resolution Forecasts of Convective Events. *Mon. Wea. Rev.*, 136, 78–97.
 764 <https://doi.org/10.1175/2007MWR2123.1>, 2008.

765 Segami, A., Kurihara, K., Nakamura, H., Ueno, M., Takano, I., and Tatsumi, Y.:
 766 Operational mesoscale weather prediction with Japan Spectral Model. *J. Meteorol.*
 767 *Soc. Jpn.*, 67, 907–924, https://doi.org/10.2151/jmsj1965.67.5_907, 1989.

768 Surcel, M., Zawadzki, I., and Yau, M. K.: On the filtering properties of ensemble
 769 averaging for storm-scale precipitation forecasts. *Mon. Wea. Rev.*, 142, 1093–1105,
 770 doi:10.1175/MWR-D-13-00134.1, 2014.

771 Surcel, M., Zawadzki, I., and Yau, M. K.: A Study on the Scale Dependence of the
 772 Predictability of Precipitation Patterns. *J. Atmos. Sci.*, 72, 216-235.
 773 <https://doi.org/10.1175/JAS-D-14-0071.1>, 2015.

774 Son, B. M. and Tan, P. V.: Experiments of heavy rainfall prediction over South of Central
 775 Viet Nam using MM5 (In Vietnamese). *Viet Nam Journal of Hydrometeorology.*,
 776 4(580), 9–18, 2009.

777 Toan, T. N., Thanh, C., Phuong, P. T., and Anh, T. V.: Assessing the predictability of WRF
 778 model for heavy rain by cold air associated with the easterly wind at high-level patterns
 779 over mid-central Viet Nam (In Vietnamese). *VNU Journal of Science: Earth and*

Environmental Sciences. v. 34, n. 1S, dec. 2018. ISSN 2588-1094.
<https://js.vnu.edu.vn/EES/article/view/4328>, 2018.

Torn, R.D., Hakim, G.J.: Initial condition sensitivity of western Pacific
extratropical transitions determined using ensemble-based sensitivity analysis. *Mon.
Weather Rev.* 137, 3388–3406. <https://doi.org/10.1175/2009MWR2879.1>, 2009.

Tsuboki, K. and Sakakibara, A.: Numerical Prediction of HighImpact Weather Systems:
The Textbook for the Seventeenth IHP Training Course in 2007, Hydrospheric
Atmospheric Research Center, Nagoya University, Nagoya, Japan, and UNESCO,
Paris, France, 273 pp., [http://www.rain.hyarc.nagoya-u.ac.jp/~tsuboki/
cress_html/src_cress/CReSS2223_users_guide_eng.pdf](http://www.rain.hyarc.nagoya-u.ac.jp/~tsuboki/cress_html/src_cress/CReSS2223_users_guide_eng.pdf) (last access: 1 May 2019),
2007.

Tuoi Tre news: [https://tuoitre.vn/mien-trung-tiep-tuc-mua-lon-14-nguoi-chet-va-mat-tich-
20181212201907413.htm](https://tuoitre.vn/mien-trung-tiep-tuc-mua-lon-14-nguoi-chet-va-mat-tich-20181212201907413.htm) (last access: 5 June 2024), 2018

Wang, C.-C.*, Kuo, H.-C., Yeh, T.-C., Chung, C.-H., Chen, Y.-H., Huang, S.-Y.,
Wang, Y.-W., and Liu, C.-H.: High-resolution quantitative precipitation forecasts and
simulations by the Cloud-Resolving Storm Simulator (CReSS) for Typhoon Morakot
(2009). *J.Hydrol.*, 506, 26-41, <http://dx.doi.org/10.1016/j.jhydrol.2013.02.018>, 2013.

Wang. C.-C.*, Lin, B.-X., Chen, C.-T., and Lo, S.-H.: Quantifying the effects of long-term
climate change on tropical cyclone rainfall using cloud-resolving models:
Examples of two landfall typhoons in Taiwan. *J. Climate*, 2015.

Wang, C.-C.: On the calculation and correction of equitable threat score for model
quantitative precipitation forecasts for small verification areas: The example of
Taiwan. *Wea. Forecasting*, 29, 788–798, doi:10.1175/WAF-D-13-00087.1, 2014.

Wang, C.-C., Huang, S.-Y., Chen, S.-H., Chang, C.-S., and Tsuboki, K.: Cloud resolving
typhoon rainfall ensemble forecasts for Taiwan with large domain and

extended range through time-lagged approach. *Wea. Forecasting*, 31,151–172,
doi:10.1175/WAF-D-15-0045.1, 2016.

Wang, C.-C., Li, M.-S., Chang, C.-S., Chuang, P.-Y., Chen, S.-H., and Tsuboki, K.:
Ensemble-based sensitivity analysis and predictability of an extreme rainfall event
over northern Taiwan in the Mei-yu season: The 2 June 2017 case. *Atmos. Res.*, 259,
105684, <https://doi.org/10.1016/j.atmosres.2021.105684>, 2021.

Wang, C.-C., Tsai, C.-H., Jou, B. J.-D., and David, S. J.: Time-Lagged Ensemble
Quantitative Precipitation Forecasts for Three Landfalling Typhoons in the Philippines
Using the CReSS Model, Part I: Description and Verification against Rain-Gauge
Observations. *Atmosphere*, 13, 1193, <https://doi.org/10.3390/atmos13081193>, 2022.

Wang, C.-C., and Nguyen, D. V.: Investigation of an extreme rainfall event during 8–12
December 2018 over central Viet Nam – Part 1: Analysis and cloud-resolving
simulation. *Nat. Hazards Earth Syst. Sci.*, 23, 771–788, <https://doi.org/10.5194/nhess-23-771-2023>, 2023.

Wang, C.-C., Chen, S.-H., Chen, Y.-H., Kuo, H.-C., Ruppert, Jr., J. H., and Tsuboki, K.:
Cloud-resolving time-lagged rainfall ensemble forecasts for typhoons in Taiwan:
Examples of Saola (2012), Soulik (2013), and Soudelor (2015). *Wea. Clim. Extremes*,
40, 100555, <https://doi.org/10.1016/j.wace.2023.100555>, 2023.

Wilks, D. S.: *Statistical Methods in the Atmospheric Sciences*. Academic Press, 648 pp.,
ISBN 13: 978-0-12-751966-1, 10: 0-12- 751966-1, 2006.

Weyn, J.A., and Durran, D.R.: The scale dependence of initial-condition sensitivities in
simulations of convective systems over the southeastern United States. *Q J R Meteorol
Soc.*,145 (Suppl.1), 57–74, <https://doi.org/10.1002/qj.3367>, 2018.

Ying, Y., and Zhang, F.: Practical and intrinsic predictability of multi-scale weather and
convectively coupled equatorial waves during the active phase of an MJO. *Journal of*

830 the Atmospheric Sciences, 74(11), 3771–3785. [https://doi.org/10.1175/JAS-D-17-](https://doi.org/10.1175/JAS-D-17-0157.1)
831 [0157.1](https://doi.org/10.1175/JAS-D-17-0157.1), 2017.

832